Hindawi
Contrast Media & Molecular Imaging
Volume 2018, Article ID 7832805, 8 pages
https://doi.org/10.1155/2018/7832805

Research Article

Evaluation of ^{99m}Tc-HYNIC-VCAM-1$_{scFv}$ as a Potential Qualitative and Semiquantitative Probe Targeting Various Tumors

Xiao Zhang,[1,2] Fan Hu,[1,2] Chunbao Liu,[1,2] Lianglan Yin,[1,2] Yingying Zhang,[1,2] Yongxue Zhang,[1,2] and Xiaoli Lan[1,2]

[1]*Department of Nuclear Medicine, Union Hospital, Tongji Medical College, Huazhong University of Science and Technology, Wuhan 430022, China*
[2]*Hubei Key Laboratory of Molecular Imaging, Union Hospital, Tongji Medical College, Huazhong University of Science and Technology, Wuhan 430022, China*

Correspondence should be addressed to Xiaoli Lan; lxl730724@hotmail.com

Received 15 January 2018; Accepted 25 March 2018; Published 3 May 2018

Academic Editor: Ya-Yao Huang

Vascular cell adhesion molecule 1 (VCAM-1) is overexpressed in varieties of cancers. This study aimed to evaluate the application of a single chain variable fragment (scFv) of anti-VCAM-1 antibody labeled with ^{99m}Tc as a possible imaging agent in several tumors. VCAM-1 scFv was labeled with ^{99m}Tc using succinimidyl 6-hydrazinium nicotinate hydrochloride, and ^{99m}Tc-HYNIC-VCAM-1$_{scFv}$ was successfully synthesized with a high radiolabeling yield. VCAM-1 expression was evaluated in six cell lines by immunofluorescence staining. In vitro binding assays showed different binding affinities of ^{99m}Tc-HYNIC-VCAM-1$_{scFv}$ in different tumor cell lines, with high uptake in B16F10 melanoma and HT1080 fibrosarcoma cells, which was consistent with immunofluorescence staining results. In vivo SPECT planar imaging demonstrated that B16F10 and HT1080 tumors could be clearly visualized. Less intense uptake was observed in human SKOV3.ip ovarian tumor, and weak uptake was observed in human A375m melanoma, MDA-MB-231 breast cancer, and 786-O renal tumors. These findings were confirmed by biodistribution and immunofluorescence studies. High uptake by B16F10 tumors was inhibited by excess unlabeled VCAM-1$_{scFv}$. ^{99m}Tc-HYNIC-VCAM-1$_{scFv}$, which selectively binds to VCAM-1, can provide a qualitative and semiquantitative method for noninvasive evaluation of VCAM-1 expression by tumors.

1. Introduction

Metastasis, one of the hallmarks of malignancy, remains a significant clinical obstacle to a favorable prognosis. Early, accurate diagnosis and targeted therapy are crucial. A prognostic tumor biomarker is very helpful for the diagnosis and targeted therapy of cancers [1]. Vascular cell adhesion molecule 1 (VCAM-1) is an immunoglobulin- (Ig-) like adhesion molecule with seven extracellular Ig domains. VCAM-1 is believed to be responsible for tumor proliferation and metastasis, and its levels correlate with prognosis [2]. It is expressed by multiple types of aggressive neoplasms, including those involving lung, prostate, breast, ovaries, and colon [3]. VCAM-1 has emerged as a target for therapy of these tumors [4]. Considering the aberrant expression of VCAM-1 in tumor biology, the development of noninvasive molecular imaging for VCAM-1 is crucial for better tumor diagnosis, prognosis, and therapy planning.

Multiple new techniques for targeting VCAM-1 have been developed in the past decades, including monoclonal antibodies, nanobodies, peptides, and single chain variable fragments (scFvs) [5–8]. As we know, intact monoclonal antibodies have strong binding affinity, but their large molecular weight leads to their slow clearance from blood and poor tissue penetration into tumors. [9]. In contrast, small peptides have the advantages of prompt excretion of unbound tracer and allow prompter imaging, but at the cost of low binding affinity [10]. Given all these considerations, small antibody

fragments of moderate size and sufficient targeting ability are becoming attractive candidates for clinical application [11].

We previously prepared the scFv of anti-VCAM-1 (VCAM-1_{scFv}) using the phage display method, which is a widely used process to obtain scFvs with high specificity [12, 13]. Due to the small molecular size (~28 kDa), scFv has the advantage of rapid clearance through renal excretion, lower concentration in liver, and stronger penetration into tumor tissues [14].

The aim of this study was to explore the possibility of a noninvasive and semiquantitative method for targeting VCAM-1 in tumors, which may allow early cancer diagnosis, more precise prognosis, and targeted treatment options. In this study, we radiolabeled VCAM-1_{scFv} with ^{99m}Tc using succinimidyl 6-hydrazinium nicotinate hydrochloride (SHNH) to detect levels of VCAM-1 in several tumor models *in vivo*.

2. Materials and Methods

2.1. ^{99m}Tc-6-Hydrazinonicotinamide- (HYNIC-) VCAM-1_{scFv} Labeling Procedure. SHNH (20 μg, 69.8 nmol, Solulink, Inc., San Diego CA, USA) was added to the scFv (78.4 μg, 28 nmol, Shanghai Raygene Biotech Company) and reacted in darkness overnight at 4°C. Afterwards, 100 μL tricine (100 mg/mL, pH 5.2, Sigma/Aldrich, St. Louis MO, USA), 4 μL $SnCl_2{\cdot}2H_2O$ (7 mg/mL, Sigma-Aldrich), and 500 μL $^{99m}TcO_4^-$ solution (555 MBq, Beijing Atom High Tech, Beijing, China) were added to the reactions and incubated for 30 min at room temperature to prepare ^{99m}Tc-HYNIC-VCAM-1_{scFv}. The product was purified using a PD-10 gel column (General Electric, Fairfield CT, USA). The radiolabeled compound was analyzed by instant thin layer chromatography (ITLC) under identical conditions to calculate its radiolabeling efficiency, radiochemical purity, and *in vitro* stability (1, 3, 6, and 12 h in fetal bovine serum [FBS] and phosphate-buffered saline [PBS], $n = 5$ per group). Fifty percent acetonitrile and 0.01 M PBS were used as the developing solvent system.

2.2. Cell Culture. B16F10 and A375m melanoma cells, SKOV3.ip human ovarian cancer cells, and MDA-MB-231 human breast cancer cells were cultured in Dulbecco's modified Eagle's medium (DMEM) (Gibco, Carlsbad CA, USA). 786-O human renal cancer cells and HT-1080 human fibrosarcoma cells were maintained in Roswell Park Memorial Institute (PRMI-1640) and Minimal Essential Medium (MEM), respectively. All of the media were supplemented with 10% FBS (Gibco, Grand Island, NY, USA), 100 U/mL penicillin, and 100 μg/mL streptomycin (Beyotime, Shanghai, China).

2.3. VCAM-1 Expression Confirmed by Immunofluorescence Staining. B16F10, HT-1080, SKOV3.ip, A375m, MDA-MB-231, and 786-O cells were digested, resuspended, and seeded in six-well plates at 1×10^6 cells/well and incubated overnight. Then the samples were fixed with 4% paraformaldehyde at room temperature for 20 min and blocked in 1% bovine serum albumin (BSA) for 1 h, followed by incubation with VCAM-1 antibody (rabbit anti-VCAM-1, diluted 1 : 200, Abcam, Cambridge, MA, USA) at 4°C overnight. The next day, after incubation with fluorescent antibody (fluorescein isothiocyanate- [FITC-] labeled goat anti-rabbit IgG, diluted 1 : 50, Aspen, Wuhan, China) at 4°C for 30 min, the cells were stained with 4-6-diamidino-2-phenylindole (DAPI) for 5 min. Finally, the samples were observed under a confocal microscope (LSM 710; Zeiss, Oberkochen, Germany).

2.4. Cell Binding Assay. The binding affinity of ^{99m}Tc-HYNIC-VCAM-1_{scFv} to B16F10, HT-1080, SKOV3.ip, A375m, MDA-MB-231, and 786-O cells was measured by a cell uptake assay. Briefly, the experiment was carried out in 24-well plates (2×10^5 cells/well) and then incubated with 0.5 mL serum-free DMEM, PRMI-1640, or MEM containing ^{99m}Tc-HYNIC-VCAM-1_{scFv} (2 nM) at 37°C for 1, 2, or 4 h, respectively. Thereafter, the cells were rinsed twice with 1 mL PBS and lysed with 1 N NaOH. The radioactivity in the cell lysate was counted using an automatic well-type gamma counter (PerkinElmer WIZARD2 2470, Shelton, CT, USA). For a blocking study, B16F10 cells were incubated with ^{99m}Tc-HYNIC-VCAM-1_{scFv} (2 nM) at 37°C for 4 h in the presence of no other VCAM-1_{scFv}, 100 nM unlabeled VCAM-1_{scFv}, or 100 nM unlabeled HYNIC-VCAM-1_{scFv}, and the radioactivity of the cell suspensions was measured.

2.5. Preparation of Tumor Models. All animal studies were performed in accordance with a protocol approved by the Institutional Animal Care and Use Committee (IACUC) of Tongji Medical College, Huazhong University of Science and Technology. Female BALB/c nude mice (3-4 weeks, Beijing HFK Bioscience Company, Beijing, China) were injected subcutaneously in the left shoulder with 5×10^6 B16F10, HT-1080, A375m, MDA-MB-231, SKOV3.ip, or 786-O cells ($n = 5$ per group), suspended in 150 μL PBS. The mice were used as models for *in vivo* SPECT planar imaging and biodistribution studies when the xenograft masses reached a size of 5 to 10 mm.

2.6. SPECT Planar Imaging. Imaging studies were performed in the tumor-bearing mice using SPECT (Symbia T6, Siemens, Erlangen, Germany) with a 3.0 mm pinhole collimator. Briefly, under isoflurane anesthesia, after intravenous injection of ^{99m}Tc-HYNIC-VCAM-1_{scFv} (7.4–11.1 MBq), images were acquired at 1, 2, and 4 h postinjection. For the blocking study, B16F10 tumor-bearing mice were given a 50-fold excess dose of unlabeled VCAM-1_{scFv} 1 h prior to the injection of ^{99m}Tc-HYNIC-VCAM-1_{scFv}. The acquisition time was 10 min for each mouse.

2.7. Biodistribution Study. For biodistribution studies, five B16F10 tumor-bearing mice were injected with ^{99m}Tc-HYNIC-VCAM-1_{scFv} (1.85 MBq) via tail vein and sacrificed at 1, 2, and 4 h postinjection. For the blocking study, B16F10 tumor-bearing mice ($n = 5$) were sacrificed at 1 h after the injection. The biological tissues of interest (i.e., blood, brain, myocardium, liver, spleen, lung, kidney, stomach, intestine, muscle, bone, and tumor) were removed, washed, and weighed, and their radioactivity was measured with decay

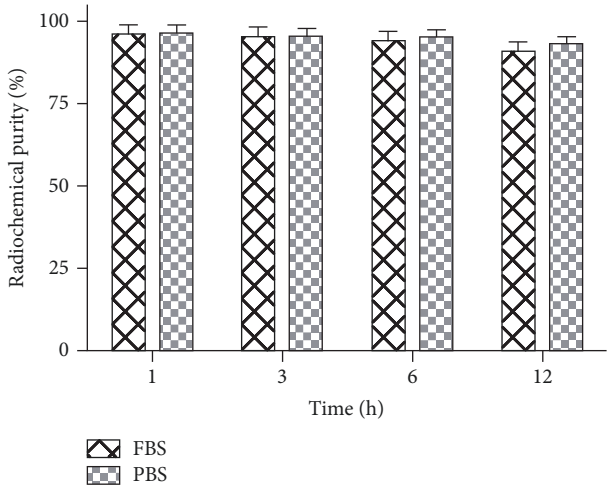

Figure 1: Stability of ^{99m}Tc-HYNIC-VCAM-1$_{scFv}$ in FBS and PBS at different time points. All data are expressed as the means ± SD (n = 5). FBS = fetal bovine serum. PBS = phosphate-buffered saline.

correction using an automatic well-type gamma counter. The uptake in the tissues was expressed as a percentage of the injected dose per gram of tissue (% ID/g). Five groups of five mice, each group grafted with one of the five other tumors, were sacrificed 4 h postinjection of ^{99m}Tc-HYNIC-VCAM-1$_{scFv}$ (1.85 MBq), and the % ID/g was calculated as described above. Portions of the tumors, livers, and kidneys in the 4 h biodistribution groups were removed to check the expression of VCAM-1 with immunofluorescence staining. The results were analyzed using ImageJ software (version 1.46r, Wayne Rasband, National Institutes of Health, Bethesda, MD, USA).

2.8. Statistical Analysis. Statistical Package for the Social Sciences (SPSS) software (version 13.0, SPSS Inc., Chicago, IL, USA) and GraphPad Prism (version 5.0, San Diego, CA, USA) were applied in statistical analysis. All data are presented as the mean ± standard deviation (SD). Means were compared using Student's t-test with $P < 0.05$ being statistically significant.

3. Results

3.1. Radiolabeling Yield, Radiochemistry, and Stability. ^{99m}Tc-HYNIC-VCAM-1$_{scFv}$ had a high radiolabeling yield of 81.5 ± 3.6% and a specific activity of 16.2 ± 1.1 MBq/nmol (n = 5). After purification, the radiochemical purity of ^{99m}Tc-HYNIC-VCAM-1$_{scFv}$ reached 96.5 ± 1.7% and was >90% at 1, 3, 6, and 12 h in FBS and PBS (Figure 1), indicating good stability *in vitro*.

3.2. VCAM-1 Expression In Vitro. The relative VCAM-1 expression levels in the cancer cell lines evaluated by immunofluorescence are shown in Figure 2. The results demonstrated strong intensities in B16F10 and HT1080 cells, a moderate intensity in SKOV3.ip cells, and low intensities in A375m, MDA-MB-231, and 786-O cells, which correlated with the VCAM-1 expression levels of these cells.

3.3. Cell Binding Assay. As shown in Figure 3(a), the uptake of ^{99m}Tc-HYNIC-VCAM-1$_{scFv}$ by B16F10 and HT1080 cells (2×10^5) increased with time and reached a plateau (6.07 ± 0.55%, 5.73 ± 0.41%) at 4 h. The accumulation of radioactivity in SKOV3.ip cells (3.40 ± 0.26%, 4 h) had a moderate increase and the binding of ^{99m}Tc-HYNIC-VCAM-1$_{scFv}$ to A375m, MDA-MB-231, and 786-O cells remained relatively stable over time (2.47 ± 0.09%, 2.67 ± 0.13%, and 2.53 ± 0.18%, 4 h). These data reveal that ^{99m}Tc-HYNIC-VCAM-1$_{scFv}$ binds strongly to B16F10 and HT1080 cells, moderately to SKOV3.ip cells, and weakly to A375m, MDA-MB-231, and 786-O cells. The blocking study (Figure 3(b)) showed that the uptake of ^{99m}Tc-HYNIC-VCAM-1$_{scFv}$ in the presence of 100 nM unlabeled HYNIC-VCAM-1$_{scFv}$ or 100 nM unlabeled VCAM-1$_{scFv}$ in B16F10 cells was much lower than their corresponding nonblocked groups at 4 h (6.07 ± 0.55%, 2.67 ± 0.12%, and 2.77 ± 0.15%, $P < 0.01$). The blocking study demonstrates the specificity of ^{99m}Tc-HYNIC-VCAM-1$_{scFv}$ for VCAM-positive cells.

3.4. SPECT Planar Imaging. B16F10 and HT1080 tumors images were clearly visualized, with high tumor-to-background contrast at all scan time points (3.20 ± 0.63, 3.90 ± 0.85, and 3.21 ± 1.05 for B16F10; 3.39 ± 0.65, 3.28 ± 0.84, and 3.13 ± 0.63 for HT1080, Figures 4(a) and 4(b)). We chose contralateral limb of the tumor as background value. Weaker uptake was observed by SKOV3.ip tumor (2.75 ± 0.57, 1 h, Figure 4(c)), and the probe uptakes in A375m, MDA-MB-231, and 786-O tumors (Figures 4(d), 4(e), and 4(f)) were indistinguishable from background (1.85 ± 0.32, 1.84 ± 0.75, and 1.77 ± 0.47, 1 h). As shown in Figure 5, the accumulation of radioactivity in B16F10 tumors clearly decreased in the presence of excess unlabeled VCAM-1. These results indicate that ^{99m}Tc-HYNIC-VCAM-1$_{scFv}$ can specifically target VCAM-1-positive tumors. In addition, the images of the kidneys and the livers were visualized clearly, which confirmed that in vivo clearance of the probe is mainly through the renal and hepatic routes.

3.5. Biodistribution Study. We also assessed tumor targeting and nontumor tissue distribution of ^{99m}Tc-HYNIC-VCAM-1$_{scFv}$ in the six tumor models (Figure 6). In B16F10 tumor models (Figure 6(a)), highest accumulation was noted in the kidneys at all time points, and the radioactivities in kidneys decreased steadily. The results indicated urinary system was the main pathway of ^{99m}Tc-HYNIC-VCAM-1$_{scFv}$ excretion. The B16F10 tumor uptakes were 5.51 ± 0.37% ID/g, 5.04 ± 0.61% ID/g, and 4.93 ± 0.52% ID/g at 1, 2, and 4 h postinjection, respectively, and tumor-to-blood (T/B) and tumor-to-muscle (T/M) ratios increased over time from 1.25 ± 0.08 and 6.68 ± 0.79 at 1 h postinjection to 1.88 ± 0.17 and 8.47 ± 1.05 at 4 h postinjection in B16F10 xenograft mice (Figure 6(c)), which bodes well for the application of ^{99m}Tc-HYNIC-VCAM-1$_{scFv}$ as an *in vivo* molecular imaging agent.

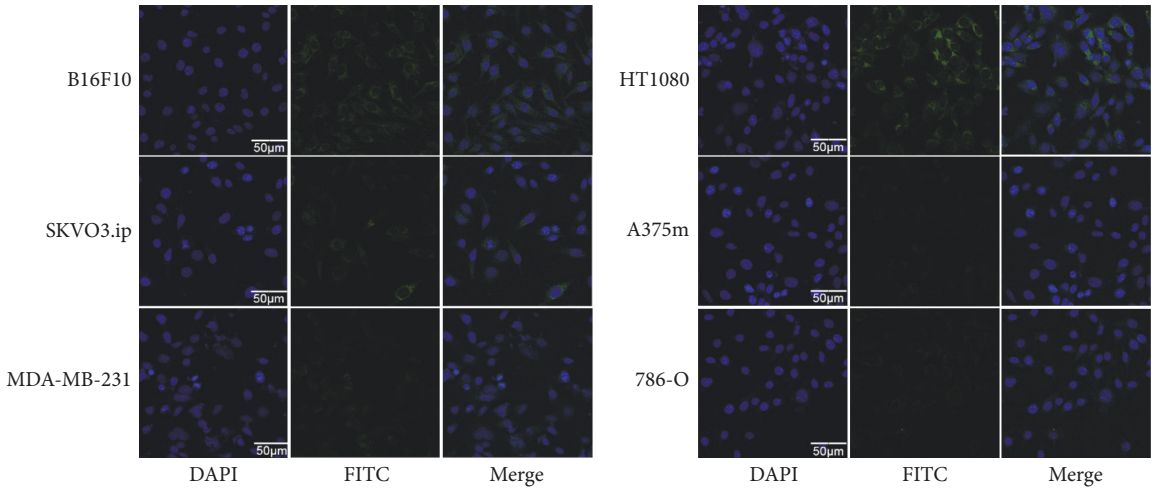

FIGURE 2: Immunofluorescence staining of six cancer cell lines. The cells were incubated with VCAM-1 antibody (green) and nuclei were stained with 4′,6-diamidino-2-phenylindole (DAPI). Representative images are displayed at the same scale (×600) ($n = 5$). DAPI = 4′,6-diamidino-2-phenylindole. FITC = fluorescein isothiocyanate.

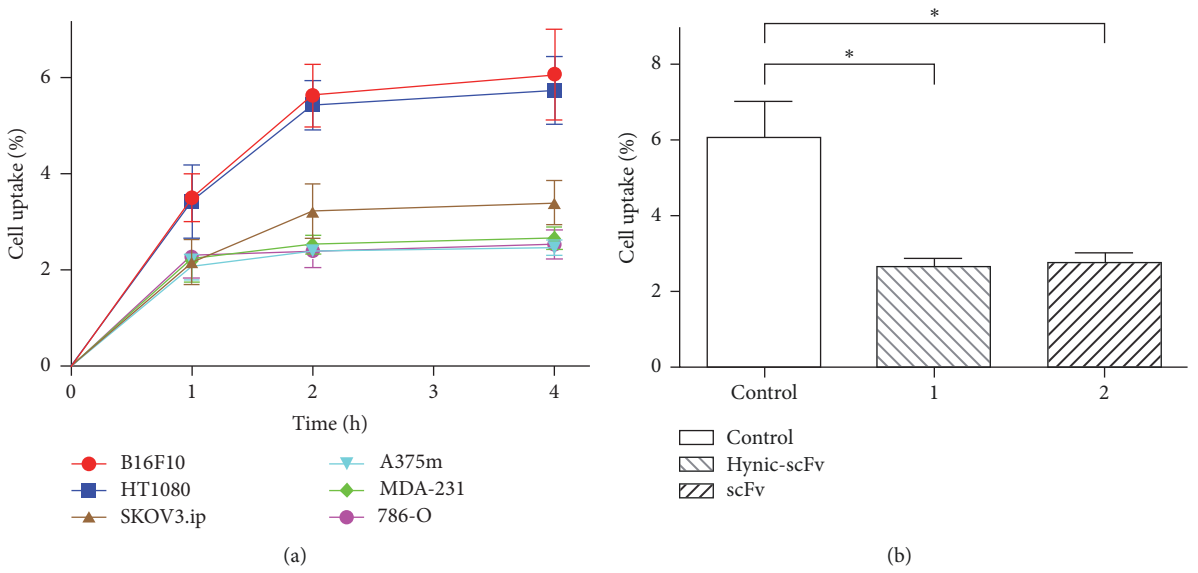

FIGURE 3: Cell uptake and blocking studies of ^{99m}Tc-HYNIC-VCAM-1$_{scFv}$ *in vitro*. The ^{99m}Tc-HYNIC-VCAM-1$_{scFv}$ (2 nM) cell uptake studies (a) were performed on a series of cancer cell lines at serial time points. The comparisons of ^{99m}Tc-HYNIC-VCAM-1$_{scFv}$ uptake in the blocking experiments (b) with no other VCAM-1$_{scFv}$, excess unlabeled VCAM-1$_{scFv}$, and HYNIC-VCAM-1$_{scFv}$. $^{*}P < 0.01$. All data are expressed as mean ± SD in triplicate.

As expected, the tumor concentration of ^{99m}Tc-HYNIC-VCAM-1$_{scFv}$ in the blocked mice was significantly lower than that in the unblocked mice (2.92 ± 0.26% ID/g versus 5.51 ± 0.37% ID/g, $P < 0.001$, Figure 6(b)) at 1 h, while the uptake in nontumor tissues was not significantly reduced by the blocking dose, suggesting that nontumor tissues did not express significant VCAM-1 and took up the tracer nonspecifically. The uptakes of ^{99m}Tc-HYNIC-VCAM-1$_{scFv}$ in HT-1080, SKOV3.ip, A375m, MDA-MB-231, and 786-O tumor models were 4.65 ± 0.39% ID/g, 2.99 ± 0.44% ID/g, 1.33±0.22% ID/g, 1.49±0.23% ID/g, and 1.47±0.31% ID/g at 4 h postinjection (Figures 6(d) and 6(e)), respectively, which were in agreement with *in vivo* images. The ratios of T/B and T/M (Figures 6(f) and 6(g)) were also similar.

As shown in Figure 7, immunofluorescence staining of the kidneys and liver showed relatively low signals, indicating that these tissues did not express VCAM-1 significantly, again showing that high uptake in the kidneys and liver was unrelated to specific binding to VCAM-1 in these organs and largely attributed to the clearance of the probe. The immunofluorescence intensities of the tumor tissues (Figure 7), which were extracted from different tumor-bearing mice of the 4 h

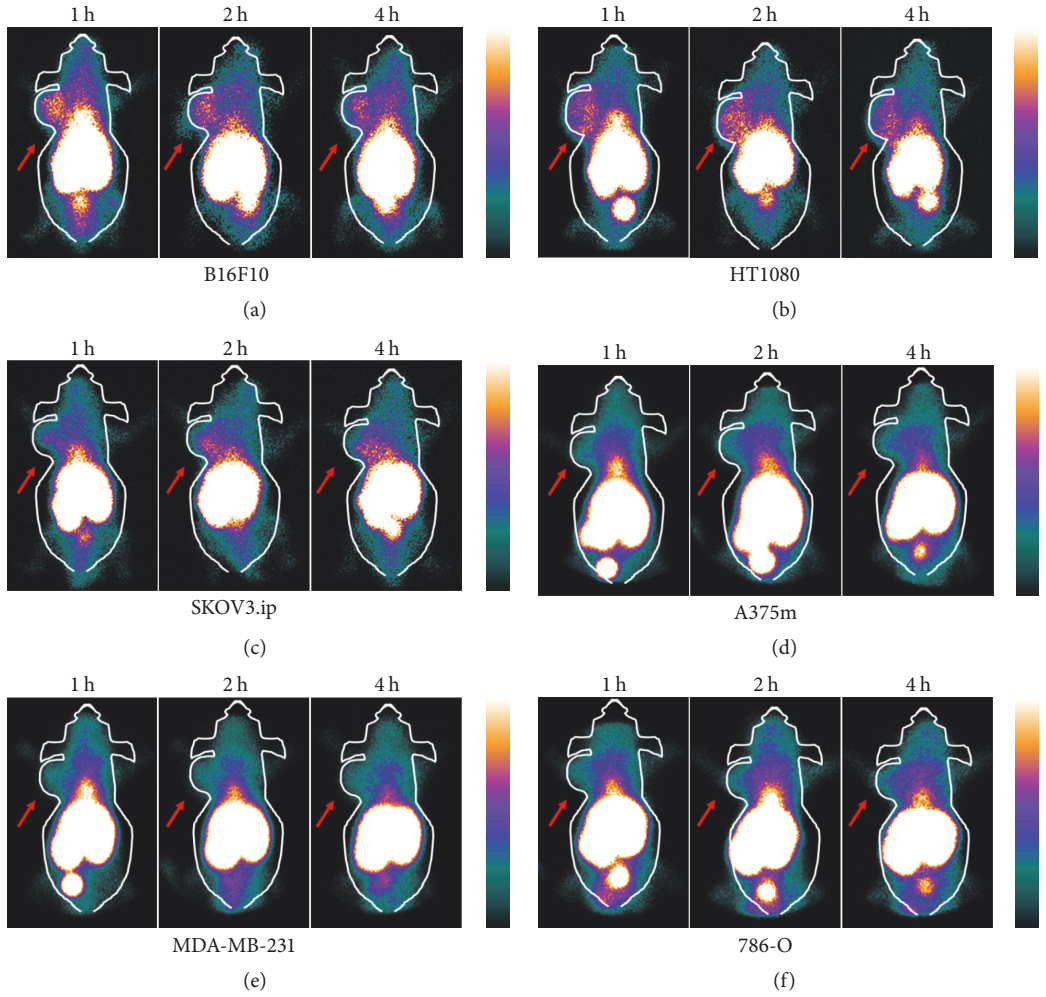

Figure 4: Representative SPECT planar imaging of ^{99m}Tc-HYNIC-VCAM-1$_{scFv}$ in six tumor models ($n = 5$ per group) obtained at 1, 2, and 4 h, respectively. Arrows refer to tumors.

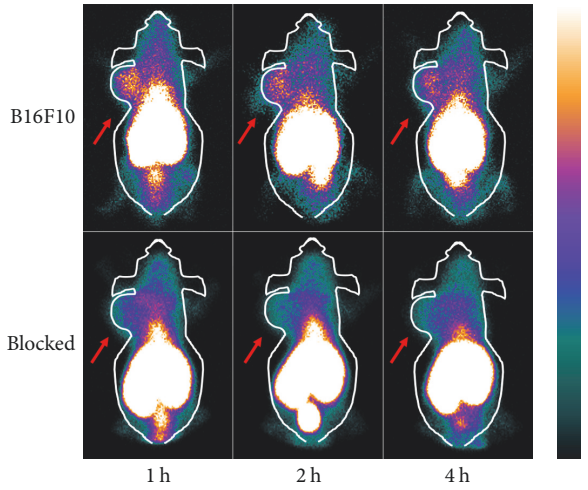

Figure 5: SPECT planar imaging of B16F10 tumor-bearing mice at the indicated time points after ^{99m}Tc-HYNIC-VCAM-1$_{scFv}$ injection, with/without preinjection of excess unlabeled VCAM-1$_{scFv}$. Arrows indicate tumors.

biodistribution groups, further validated the different VCAM-1 expression levels of six tumor models. ^{99m}Tc-HYNIC-VCAM-1$_{scFv}$ accumulation in the tumors significantly correlated well with average integral optical density of VCAM-1 expression (Figure 8, $R^2 = 0.875$, $P < 0.0001$), which suggested the possibility of semiquantitative evaluation for VCAM-1 noninvasively *in vivo*.

4. Discussion

Recently, strategies for targeting VCAM-1 [5–8], such as ^{18}F labeled nanobodies and ^{111}In labeled peptides, have been investigated. VCAM-1 expressed in atherosclerosis has been the main target of research. For the availability and low costs, ^{99m}Tc is an ideal radionuclide for radiopharmaceutical synthesis and has been used more widely than ^{18}F and ^{111}In in clinical applications. Therefore, we used ^{99m}Tc-HYNIC-VCAM-1$_{scFv}$ to target VCAM-1 in various tumors to assess the binding affinity and characteristics of VCAM-1$_{scFv}$.

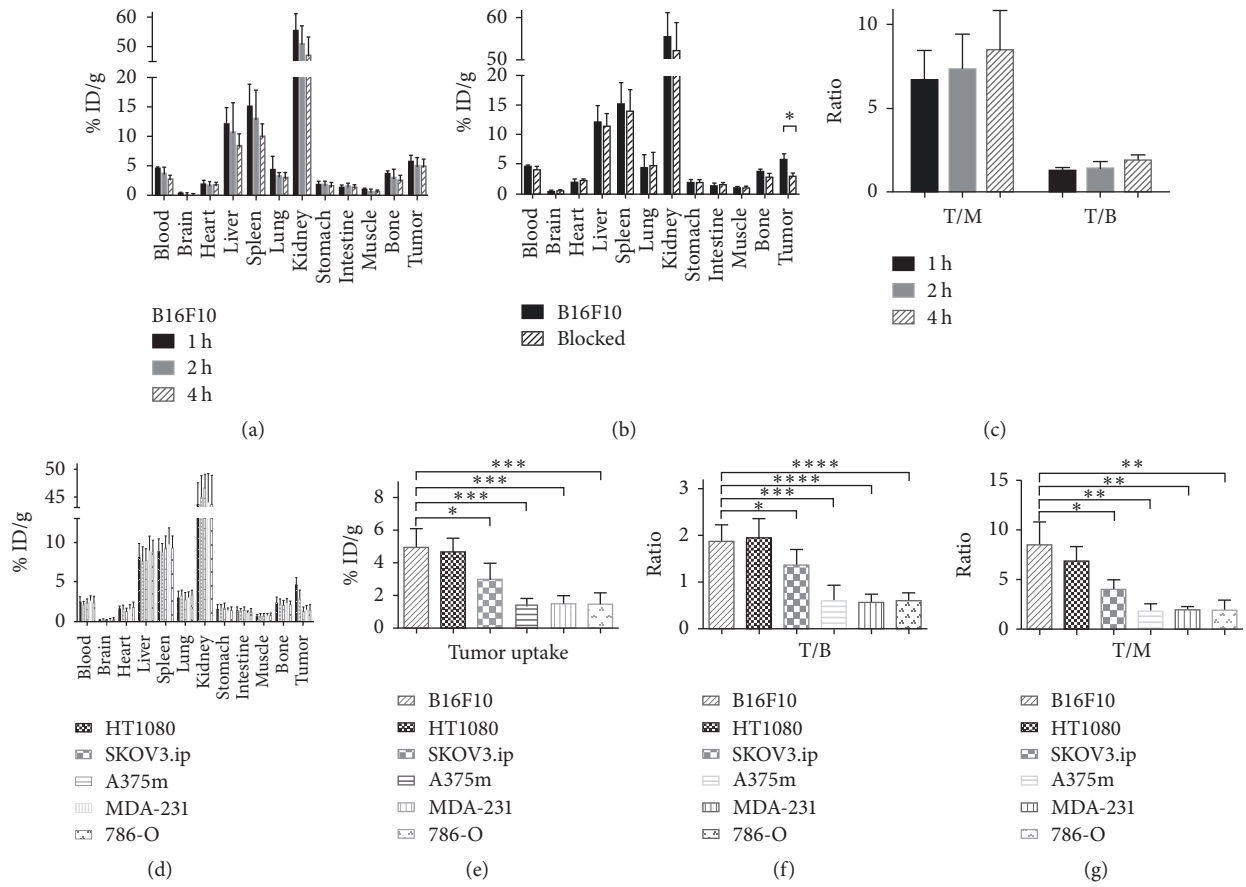

Figure 6: Tissue biodistribution of ^{99m}Tc-HYNIC-VCAM-1$_{scFv}$ in tumor xenografts. Biodistribution of ^{99m}Tc-HYNIC-VCAM-1$_{scFv}$ was assessed in mice bearing B16F10 tumors at 1, 2, and 4 h postinjection ((a), $n = 5$). The blocking study with excess VCAM-1$_{scFv}$ was performed at 1 h after ^{99m}Tc-HYNIC-VCAM-1$_{scFv}$ injection in B16F10 tumor-bearing mice (b). Tumor-to-blood (T/B) and tumor-to-muscle (T/M) ratios in mice bearing B16F10 tumors at the indicated time points (c). Biodistribution was similarly examined in five tumor models at 4 h postinjection (d). The comparison of tumor uptake (e), T/B (f), and T/M (g) in the different tumors. $^{*}P < 0.05$, $^{**}P < 0.01$, $^{***}P < 0.001$, and $^{****}P < 0.0001$.

^{99m}Tc has a half-life of 6 h, which is well matched with the relatively short physiological blood half-life of VCAM-1$_{scFv}$, making the probe's clinical translation feasible in future [15]. In addition, HYNIC-NHS, as a bifunctional chelating agent, participates in the radiolabeling of ^{99m}Tc with peptides or antibodies, which is easily prepared, with a high radiolabeling yield, radiochemical purity, and stability [16, 17]. As an alternative to PET, we sought to evaluate the feasibility of a ^{99m}Tc-HYNIC-VCAM-1$_{scFv}$ as a SPECT tracer to target VCAM-1, which is much cheaper and more easily available. In the uptake studies, six cell lines with different VCAM-1 expression levels confirmed by immunofluorescence staining showed corresponding binding affinities of the radiolabeled VCAM-1$_{scFv}$. The uptake value in B16F10 cells (VCAM-1 positive) was effectively blocked by an excess of unlabeled VCAM-1$_{scFv}$, further verifying the specificity of ^{99m}Tc-HYNIC-VCAM-1$_{scFv}$ to VCAM-1 *in vitro*.

The uptake pattern and blocking studies in the different cell lines closely correlated with the SPECT planar imaging and biodistribution study of xenograft models. In the imaging of B16F10 and HT1080 xenograft mice, tumors were visualized clearly from normal tissues as early as 1 h after injection of ^{99m}Tc-HYNIC-VCAM-1$_{scFv}$. Based on the high tissue penetrability of small antibody fragments, the probe can reach the tumor site more quickly [18]. It is significantly different from tumor imaging with intact monoclonal antibodies, mainly due to slow clearance of the larger tracers from the blood pool [19]. Moderate uptake was seen in SKOV3.ip tumors, measuring 2.99 ± 0.44% ID/g at 4 h. In contrast with VCAM-1-^{111}In peptide distribution in omentum of SKOV3ip1 cells (about 2% ID/g), ^{99m}Tc-HYNIC-VCAM-1$_{scFv}$ has a relatively higher binding affinity with SKOV3.ip tumors [8]. No obvious tracer uptake could be seen in the imaging of A375m, MDA-MB-231, and 786-O tumor models, which are consistent with the lack of VCAM-1 expression in these tumor tissues and also confirmed by immunofluorescence staining of the tissues. High T/M ratios in B16F10 and HT1080 xenografts (8.47 ± 1.05 and 6.89 ± 0.64) were observed at 4 h postinjection, showing ideal contrast for imaging of these tumors. These results suggest the targeting ability and specificity of the probe *in vivo*.

As the main excretory organs, the kidneys showed the highest accumulation in the biodistribution study, which is in agreement with Broisat et al. [20]. This is due to the small

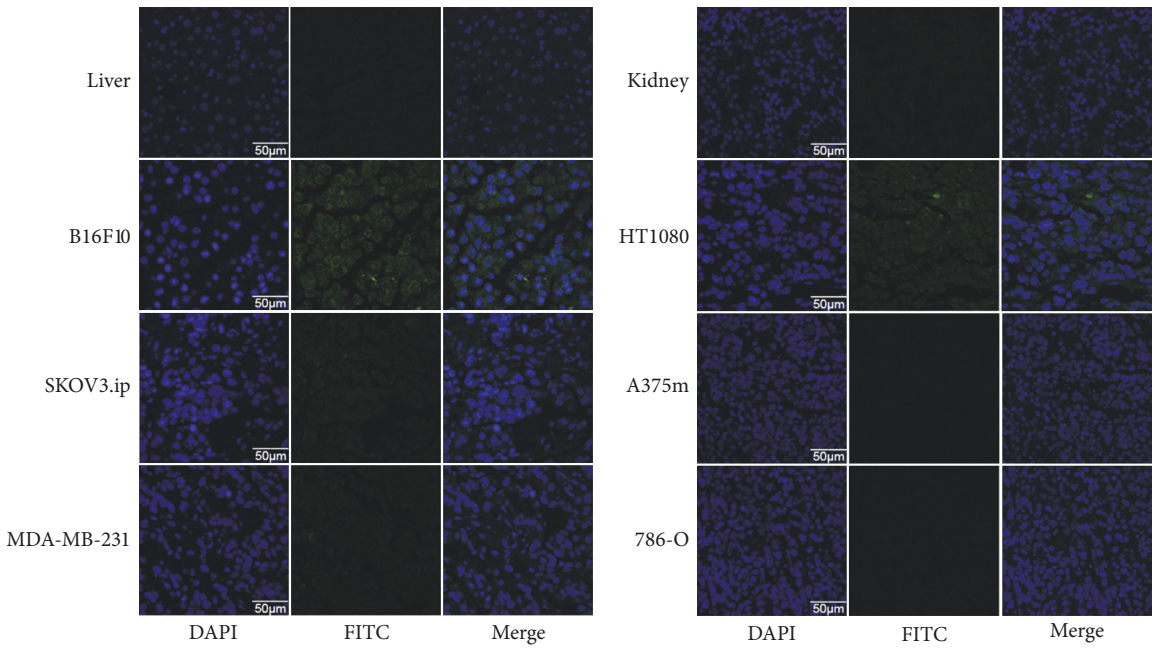

Figure 7: Immunofluorescence staining of kidneys, livers, and various tumors. The tissues were incubated with VCAM-1 antibody (green), followed by staining with DAPI. Representative images are displayed at the same scale (×600, $n = 5$).

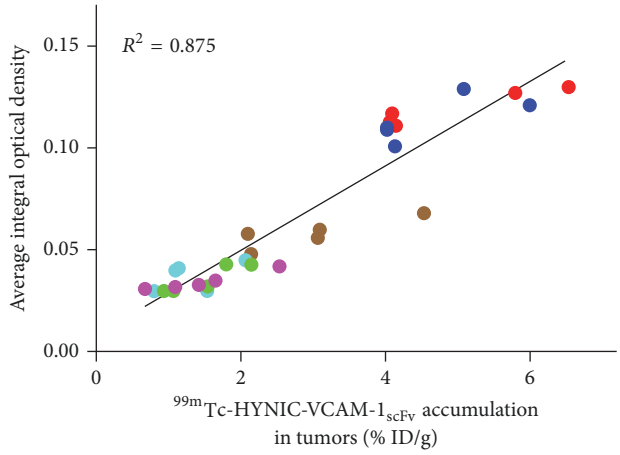

Figure 8: Relationship between the tumor uptake and mean integral optical density of VCAM-1 expression ($n = 5$ per group).

molecular weight (~28 kDa) of scFv, which is below the cut-off for renal clearance. Immunofluorescence staining showed liver and kidneys do not express significant VCAM-1, demonstrating that the accumulations in the kidneys and livers is mainly related to the excretion mode. The immunofluorescence intensity of VCAM-1 has a relationship with the radioactivity accumulated in tumors, which indicates the feasibility of achieving semiquantitative evaluation of VCAM-1 expression *in vivo*.

There are various methods to detect protein expression using molecular biological techniques [21], such as immunohistochemistry, immunofluorescence, western blotting, and ELISA. Among them, ELISA is mainly applied for the detection of secretory proteins [22]. Although the specificity of western blotting is high, the procedure is complex. This research focuses on the study of immunofluorescence and radioimmunoassay, which are both based on the antigen-antibody reaction. VCAM-1 expression detected by ^{99m}Tc-HYNIC-VCAM-1$_{scFv}$ relies on the binding of the radioactive antibody fragment (VCAM-1$_{scFv}$) with the antigen. After the binding, the radioactivity uptake is measured to quantitate the antigen expression [23]. This technique is easy to perform with high sensitivity. Immunofluorescence, which makes use of labeling antibodies with fluorescent substances, has gained more and more attention due to its high sensitivity and superiority of obtaining anatomic and physiological information. However, it needs to get specimen which is invasive and hard to repeat in the living body, and it also has some shortcomings, such as inadequate penetration depth [24]. In contrast, PET and SPECT imaging with the ability to image the living human body deeply, are more advantageous in clinical applications. The results of immunofluorescence in our study are consistent with radioimmunoassay, indicating that ^{99m}Tc-HYNIC-VCAM-1$_{scFv}$ has the potential to be used to detect VCAM-1 noninvasively and repeatedly *in vitro* and *in vivo*.

There are several issues that need to be pointed out in this study. First, high activity in blood was also observed, which renders T/B ratios (1.25 ± 0.08) not ideal in VCAM-1 positive tumor models at 1 h. Fortunately, the accumulation in blood decreased rapidly (from 4.54 ± 0.13% ID/g at 1 h to 2.67 ± 0.32% ID/g at 4 h) and the T/B value increased steadily. Second, although lower accumulation was seen in liver than that with intact monoclonal antibodies [25], the liver retained high amounts of activity after ^{99m}Tc-HYNIC-VCAM-1$_{scFv}$ administration. This will interfere with imaging of lesions in

the liver and surrounding tissues. Further studies will focus on modifying and optimizing the probe to minimize its blood and liver accumulation.

5. Conclusion

We successfully labeled an scFv-based probe, ^{99m}Tc-HYNIC-VCAM-1$_{scFv}$, that specifically binds to VCAM-1. We identified different expression levels of VCAM-1 with SPECT planar imaging of corresponding tumor lesions, which potentially provides a qualitative and semiquantitative method for non-invasive evaluation of VCAM-1 expression *in vivo*.

Conflicts of Interest

The authors declare no potential conflicts of interest.

Acknowledgments

This work was supported by the National Natural Science Foundation of China (nos. 81630049 and 81771863).

References

[1] E. Andreopoulou and M. Cristofanilli, "Circulating tumor cells as prognostic marker in metastatic breast cancer," *Expert Review of Anticancer Therapy*, vol. 10, no. 2, pp. 171–177, 2010.

[2] F. Tas, S. Karabulut, M. Serilmez, R. Ciftci, and D. Duranyildiz, "Clinical significance of serum epithelial cell adhesion molecule (EPCAM) and vascular cell adhesion molecule-1 (VCAM-1) levels in patients with epithelial ovarian cancer," *Tumor Biology*, vol. 35, no. 4, pp. 3095–3102, 2014.

[3] M. Schlesinger and G. Bendas, "Vascular cell adhesion molecule-1 (VCAM-1) - An increasing insight into its role in tumorigenicity and metastasis," *International Journal of Cancer*, vol. 136, no. 11, pp. 2504–2514, 2015.

[4] Q. Chen and J. Massagué, "Molecular pathways: VCAM-1 as a potential therapeutic target in metastasis," *Clinical Cancer Research*, vol. 18, no. 20, pp. 5520–5525, 2012.

[5] B. A. Kaufmann, C. L. Carr, J. T. Belcik et al., "Molecular imaging of the initial inflammatory response in atherosclerosis: Implications for early detection of disease," *Arteriosclerosis, Thrombosis, and Vascular Biology*, vol. 30, no. 1, pp. 54–59, 2010.

[6] C. Liu, X. Zhang, Y. Song et al., "SPECT and fluorescence imaging of vulnerable atherosclerotic plaque with a vascular cell adhesion molecule 1 single-chain antibody fragment," *Atherosclerosis*, vol. 254, pp. 263–270, 2016.

[7] G. Bala, A. Blykers, C. Xavier et al., "Targeting of vascular cell adhesion molecule-1 by 18F-labelled nanobodies for PET/CT imaging of inflamed atherosclerotic plaques," *European Heart Journal—Cardiovascular Imaging*, vol. 17, no. 9, pp. 1001–1008, 2016.

[8] J. M. Scalici, S. Thomas, C. Harrer et al., "Imaging VCAM-1 as an indicator of treatment efficacy in metastatic ovarian cancer," *Journal of Nuclear Medicine*, vol. 54, no. 11, pp. 1883–1889, 2013.

[9] Y. Liu, X. Jin, X. Lan, J. Lang, Q. Wen, and R. An, "SPECT imaging of colorectal cancer by targeting CD133 receptor with 99mTc-labeled monoclonal antibody," *The Quarterly Journal of Nuclear Medicine and Molecular Imaging*, 2016.

[10] C. Li, H. Feng, X. Xia et al., "99mTc-labeled tetramer and pentamer of single-domain antibody for targeting epidermal growth factor receptor in xenografted tumors," *Journal of Labelled Compounds and Radiopharmaceuticals*, vol. 59, no. 8, pp. 305–312, 2016.

[11] C. Li, Y. Zhang, L. Wang et al., "A novel multivalent ^{99m}Tc-labeled EG2-C4bpα antibody for targeting the epidermal growth factor receptor in tumor xenografts," *Nuclear Medicine and Biology*, vol. 42, no. 6, pp. 547–554, 2015.

[12] C. M. Hammers and J. R. Stanley, "Antibody phage display: technique and applications.," *Journal of Investigative Dermatology*, vol. 134, no. 2, p. e17, 2014.

[13] A. K. Iyer, X. Lan, X. Zhu et al., "Novel human single chain antibody fragments that are rapidly internalizing effectively target epithelioid and sarcomatoid mesotheliomas," *Cancer Research*, vol. 71, no. 7, pp. 2428–2432, 2011.

[14] S. K. Sharma, M. Wuest, J. D. Way, V. R. Bouvet, M. Wang, and F. R. Wuest, "Synthesis and pre-clinical evaluation of an (18)F-labeled single-chain antibody fragment for PET imaging of epithelial ovarian cancer," *American Journal of Nuclear Medicine and Molecular Imaging*, vol. 6, no. 3, pp. 185–198, 2016.

[15] F. Li, T. Cheng, Q. Dong et al., "Evaluation of 99mTc-HYNIC-TMTP1 as a tumor-homing imaging agent targeting metastasis with SPECT," *Nuclear Medicine and Biology*, vol. 42, no. 3, pp. 256–262, 2015.

[16] L. K. Meszaros, A. Dose, S. C. G. Biagini, and P. J. Blower, "Synthesis and evaluation of analogues of HYNIC as bifunctional chelators for technetium," *Dalton Transactions*, vol. 40, no. 23, pp. 6260–6267, 2011.

[17] J. D. G. Correia, A. Paulo, P. D. Raposinho, and I. Santos, "Radiometallated peptides for molecular imaging and targeted therapy," *Dalton Transactions*, vol. 40, no. 23, pp. 6144–6167, 2011.

[18] P. P. Monnier, R. J. Vigouroux, and N. G. Tassew, "In vivo applications of single chain Fv (variable domain) (scFv) fragments," *Antibodies*, vol. 2, no. 2, pp. 193–208, 2013.

[19] J. Lang, X. Lan, Y. Liu et al., "Targeting cancer stem cells with an ^{131}I-labeled anti-AC133 monoclonal antibody in human colorectal cancer xenografts," *Nuclear Medicine and Biology*, vol. 42, no. 5, pp. 505–512, 2015.

[20] A. Broisat, J. Toczek, L. S. Dumas et al., "99mTc-cAbVCAM1-5 imaging is a sensitive and reproducible tool for the detection of inflamed atherosclerotic lesions in mice," *Journal of Nuclear Medicine*, vol. 55, no. 10, pp. 1678–1684, 2014.

[21] X. Ying and T. M. Monticello, "Modern Imaging Technologies in Toxicologic Pathology: An Overview," *Toxicologic Pathology*, vol. 34, no. 7, pp. 815–826, 2006.

[22] L. E. Ott and S. Carson, "Immunological tools: Engaging students in the use and analysis of flow cytometry and enzyme-linked immunosorbent assay (ELISA)," *Biochemistry and Molecular Biology Education*, vol. 42, no. 5, pp. 382–397, 2014.

[23] V. A. Lennon, S. Whittingham, P. R. Carnegie, T. A. McPherson, and I. R. Mackay, "Detection of antibodies to the basic protein of human myelin by radioimmunoassay and immunofluorescence.," *The Journal of Immunology*, vol. 107, no. 1, pp. 56–62, 1971.

[24] G. Hong, J. T. Robinson, Y. Zhang et al., " In Vivo Fluorescence Imaging with Ag ," *Angewandte Chemie*, vol. 124, no. 39, pp. 9956–9959, 2012.

[25] Z. Liu, T. Ma, H. Liu et al., "177Lu-labeled antibodies for EGFR-targeted SPECT/CT imaging and radioimmunotherapy in a preclinical head and neck carcinoma model," *Molecular Pharmaceutics*, vol. 11, no. 3, pp. 800–807, 2014.